Investigation of nonlinear absorption processes with femtosecond light pulses in lithium niobate crystals

O. Beyer,* D. Maxein, and K. Buse

Institute of Physics, University of Bonn, Wegelerstr. 8, D-53115 Bonn, Germany

B. Sturman

Institute of Automation and Electrometry, 630090 Novosibirsk, Russia

H. T. Hsieh and D. Psaltis

Department of Electrical Engineering, California Institute of Technology, Pasadena, California 91125, USA

(Received 20 December 2004; published 10 May 2005)

The propagation of high-power femtosecond light pulses in lithium niobate crystals ($LiNbO_3$) is investigated experimentally and theoretically in collinear pump-probe transmission experiments. It is found within a wide intensity range that a strong decrease of the pump transmission coefficient at wavelength 388 nm fully complies with the model of two-photon absorption; the corresponding nonlinear absorption coefficient is $\beta_p \simeq 3.5$ cm/GW. Furthermore, strong pump pulses induce a considerable absorption for the probe at 776 nm. The dependence of the probe transmission coefficient on the time delay Δt between probe and pump pulses is characterized by a narrow dip (at $\Delta t \simeq 0$) and a long (on the picosecond time scale) lasting plateau. The dip is due to direct two-photon transitions involving pump and probe photons; the corresponding nonlinear absorption coefficient is $\beta_r \simeq 0.9$ cm/GW. The plateau absorption is caused by the presence of pump-excited charge carriers; the effective absorption cross section at 776 nm is $\sigma_r \simeq 8 \times 10^{-18}$ cm^2. The above nonlinear absorption parameters are not strongly polarization sensitive. No specific manifestations of the relaxation of hot carriers are found for a pulse duration of $\simeq 0.24$ ps.

I. INTRODUCTION

Femtosecond high-power light pulses have become increasingly important in the physics of light-matter interactions. A crucial advantage of such pulses is the possibility to deposit rapidly and precisely light energy in solids. A direction of femtosecond studies is the characterization of carrier and phonon dynamics in *semiconductors* [1–3]. The fundamental items include here momentum and energy relaxation, the carrier-carrier scattering, intervalley transitions, and carrier diffusion. Various experimental methods have been developed for probing ultrafast dynamics [1]. They include pump-and-probe techniques, streak cameras, and optical Kerr gates. Numerous publications (see [4,5] and references therein) deal with the determination of Kerr and two-photon absorption coefficients in *wide-gap optical materials*.

Ferroelectric crystals, such as $LiNbO_3$, $BaTiO_3$, and $KNbO_3$, hold an intermediate position between wide-gap materials (glasses) and semiconductors with respect to the value of the forbidden gap. They are transparent in the visible and an interplay between nonlinear effects of a different nature should take place with increasing light intensity. These include the instantaneous $\chi^{(2)}$ and $\chi^{(3)}$ nonlinearities, two-photon absorption, and inertial free-carrier and photorefractive nonlinearities. A physical picture of nonlinear phenomena in the femtosecond pulse range is practically absent.

The data on electron transitions and charge transport, accumulated in continuous-wave and long-pulse holographic experiments (see, e.g. [6–11]), form a background for femtosecond studies.

In this paper we present the results of our experimental and theoretical studies of the light-induced processes in *lithium niobate* ($LiNbO_3$) crystals on the subpicosecond ($\simeq 10^{-13}$ s) time scale. The choice of this material is not accidental. It is of prime importance for various nonlinear and photorefractive applications including frequency conversion, optical parametric oscillation, holographic data storage, and domain engineering (see, e.g., [12–18]).

Information about the response of $LiNbO_3$ crystals to high-power light pulses, available in the literature, is scarce. The literature values of the two-photon absorption coefficient β range over more than one order of magnitude at the same wavelength (≈ 530 nm) [19]. These results were obtained utilizing nanosecond and subnanosecond light pulses. Most probably, the large scatter of the data is caused by systematic errors resulting from additional absorption effects from excited charge carriers that are unavoidable for long high-power pulses [5]. These processes are known to be very important for lithium niobate [20]. The only available literature data of the Kerr coefficient $n^{(2)}$ refer to the wavelength $\lambda = 532$ nm [4]; it was also obtained with the use of long pulses.

II. EXPERIMENTAL ARRANGEMENT

In our experiments we use a pump-and-probe technique. An axially symmetric pulse at the wavelength $\lambda_r = 776$ nm is

---

*Electronic address: beyer@physik.uni-bonn.de; URL: www.physik.uni-bonn.de/hertz
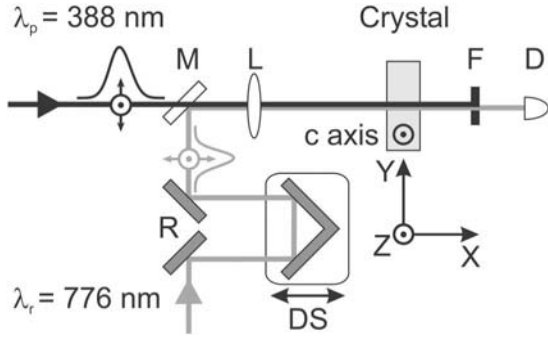
FIG. 1. Schematic diagram of a collinear pump-probe experiment; M is a dichroic mirror, L is a long-focus (500 mm) lens, F is a band edge filter for the pump light, D is a photodetector, DS is a probe delay stage, and R are reflectors.

obtained from a Ti:sapphire amplified laser system CPA-2010, Clark-MXR, Inc. The temporal full width at half maximum (FWHM) of the pulse intensity is $\simeq 0.24$ ps. About 4% of the pulse energy is tapped and serves as the incident probe. The rest of the pulse is passed through a 1-mm-thick BBO (β-BaB$_2$O$_4$) crystal to generate a pump pulse at the wavelength $\lambda_p = 388$ nm. The remaining 776 nm light in the pump beam is blocked with the help of dielectric filters.

The experimental setup is shown schematically in Fig. 1. Pump and probe pulses are incident normally and collinearly onto the YZ face of a LiNbO$_3$ sample. The arrival time of the probe pulse can be tuned by a variable-delay stage. The polar **c** axis of the sample is parallel to the Z axis. The input polarization vector of the pump pulse is either parallel or perpendicular to the **c** axis. The spatial FWHM of the pulses at the input face is about 0.6 mm. The peak intensity of the pump pulse I_p^0 ranges from $\simeq 1$ to $\simeq 276$ GW/cm^2. The maximum pump pulse fluence is about 59 mJ/cm^2. The output energy of the pump and probe pulses can be measured separately by a photodetector.

The difference in the wavelengths λ_r and λ_p enables us to separate easily the transmitted pump and probe signals. On the other hand, the collinear propagation of the pump and probe pulses simplifies the modelling procedures.

Four different samples of LiNbO$_3$, labeled as 1, 2, 3, and 4, are used in our experiments. The values of the thickness d for them are 1, 0.5, 0.07, and 0.07 mm, respectively. Samples 1, 2, and 3 are nominally undoped and possess very small ($\alpha_0 \lesssim 0.1$ cm^{-1}) linear absorption coefficients at 388 and 776 nm. Sample 4 is iron doped; the iron concentration c_{Fe} is about 5.6×10^{19} cm^{-3} and the linear absorption coefficient α_0 at 388 nm is about 15 cm^{-1}. For all the samples and wavelengths used, the linear absorption is negligibly small— i.e., $\alpha_0 d \ll 1$.

III. PUMP-PULSE PROPAGATION UNDER STRONG TWO-PHOTON ABSORPTION

Figure 2 shows the pump transmission coefficient T_p—i.e., the fraction of the fs pulse that is transmitted. In this experiment just single pulses of 388 nm wavelength are employed. The T_p values are plotted versus the peak pump pulse
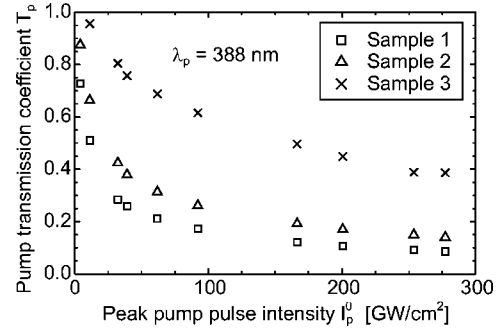

FIG. 2. Transmission coefficient T_p versus peak pump pulse intensity I_p^0. The squares, triangles, and crosses correspond to samples 1, 2, and 3, respectively.

intensity I_p^0. It is obvious that the pulses are strongly absorbed for high incident intensities. In the following we will see whether these data can be explained assuming that two-photon absorption is the dominating process.

The relevant light absorption coefficient is $\alpha_p = \beta_p I_p$, where I_p is the pump intensity and β_p is the quadratic absorption coefficient at the pump wavelength λ_p; linear absorption is supposed to be negligible.

In the actual case (see Fig. 1), the pump intensity obeys the one-dimensional nonlinear wave equation

$$\left(\frac{\partial}{\partial x} + \frac{1}{v_p} \frac{\partial}{\partial t} \right) I_p = -\beta_p I_p^2, \tag{1}$$

where x is the propagation coordinate and $v_p = c/n_p$ is the pulse velocity with n_p being the relevant refractive index. This equation follows from Maxwell's equations under the assumptions of negligible diffraction divergence and frequency dispersion, which are well justified for our experimental conditions. It has to be supplemented by a boundary condition at the input face $x=0$. Here we use a Gaussian input profile

$$I_p(x=0) = I_p^0 \exp[-(t/t_p)^2 - (r/r_p)^2], \tag{2}$$

where I_p^0 is the input peak intensity and $r = (y^2 + z^2)^{1/2}$ is the radial coordinate while r_p and t_p characterize the pump beam radius and the temporal half-width.

One can check straightforwardly that the solution of Eq. (1) meeting the boundary condition (2) is given by

$$\frac{I_p^0}{I_p} = \beta_p I_p^0 x + \exp\left[\frac{(t - x v_p^{-1})^2}{t_p^2} + \frac{r^2}{r_p^2} \right]. \tag{3}$$

This relation describes the propagation of the pump pulse with the velocity v_p, the decrease of the peak intensity, and the change of the spatiotemporal profile. The combination $x - v_p t$ that enters this relation can be considered as the spatial variable in the coordinate frame moving with the pulse velocity v_p. By setting $r=0$ and $v_p t = x$ one finds that the peak intensity decreases as $(1 + \beta_p I_p^0 x)^{-1}$ with increasing propagation distance x. By setting $v_p t = x$ we find out how the transverse beam profile is changing with increasing $\beta_p I_p^0 x$ product (see Fig. 3).
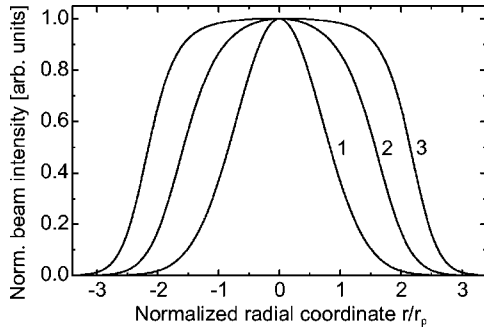
FIG. 3. Transverse beam profile (normalized intensities) for different values of the product $\beta_p I_p^0 x$. Lines 1, 2, and 3 are plotted for $\beta_p I_p^0 x = 0$ (the input shape), 10, and 100.

A strong flattening of the top of the pulse is evident; it is caused by the preferential light absorption at the beam center. The same flattening takes place for the temporal shape of the pulse at $r=0$.

Next we calculate the main measurable characteristic of the pump transmission—the normalized transmission coefficient T_p. It is defined as the ratio of the output pulse energy, measured by the photodetector (see Fig. 1), to the input pulse energy (reflections from the input and output faces can, when necessary, be taken into account). By integrating the output intensity $I_p(d,r,t)$ over the time and the transverse coordinates y,z and dividing the quantity calculated by its value at $d=0$, we obtain

$$T_p = \frac{2}{q_p \sqrt{\pi}} \int_0^\infty \ln(1 + q_p e^{-s^2}) ds. \qquad (4)$$

The transmission coefficient depends only on a single nonlinear absorption parameter $q_p = \beta_p I_p^0 d$; for $q_p = 0$ and ∞, we have $T_p = 1$ and 0, respectively. The solid line in Fig. 4 shows the calculated dependence $T_p(q_p)$. After a rapid initial fall, the further decrease of T_p occurs very slowly; this is indeed due to the relatively weak energy absorption at the pulse wings. Even for an extremely high nonlinear absorption pa-
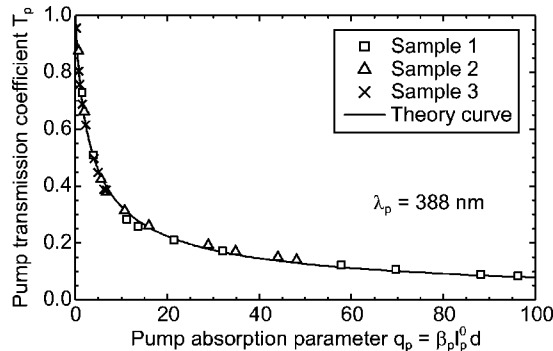
rameter $q_p = 100$, about 8% of the incident energy is passing through.

Now we turn back to the experimental results shown in Fig. 2. In Fig. 4 they are shown again, but now plotted versus the dimensionless pump absorption parameter $q_p = \beta_p I_p^0 d$. The only variable parameter to fit the characteristic theoretical curve to all experimental data is the two-photon absorption coefficient β_p. An excellent agreement between theory and experiment for all three samples within the large intensity range is evident. This proves unambiguously that two-photon absorption is the reason for the pump attenuation.

The value of the two-photon absorption coefficient at 388 nm deduced from our experiment is $\beta_p \simeq 3.5$ cm/GW. The maximum value of the product $\beta_p I_p^0 d$ is about 96, 48, and 7 for samples 1, 2, and 3, respectively; the pump pulse is subjected to a strong nonlinear absorption even in the relatively thin samples.

In the general case, the nonlinear absorption coefficient β_p is expected to be different for the Z- and Y-polarized pump beam. Our experiments have shown, however, that the corresponding difference is fairly small, less than 15%.

By varying the pump wavelength, it is possible to measure the dependence $\beta_p(\lambda_p)$. The corresponding data for the range (388–776 nm) are presented elsewhere [21]. As might be expected, the absorption coefficient β_p is strongly decreasing with increasing pump wavelength; it tends to zero when approaching the upper boundary of the above spectral interval.

Having understood the nonlinear pump propagation, we can now turn to studies of the influence of the pump on the probe pulse propagation.

IV. PROBE TRANSMISSION VERSUS PUMP-PROBE DELAY TIME

A. Experimental data

Figure 5 shows the dependence of the probe transmission coefficient T_r at $\lambda_r = 776$ nm on the time delay Δt between readout (probe) and pump pulses on the picosecond time scale for sample 4 ($d=0.07$ mm) and four different values of the pump intensity; both pulses are Y polarized (ordinary waves). In all experimental curves Δt is defined to be zero when T_r reaches the smallest value.

FIG. 4. Dependence of the transmission coefficient T_p on $\beta_p I_p^0 d$. The solid line (characteristic curve) is calculated from Eq. (4). The squares, triangles, and crosses represent the experimental data on $T_p(I_p^0 d)$, scaled by a factor of $\beta_p = 3.5$ cm/GW, for samples 1, 2, and 3, respectively.
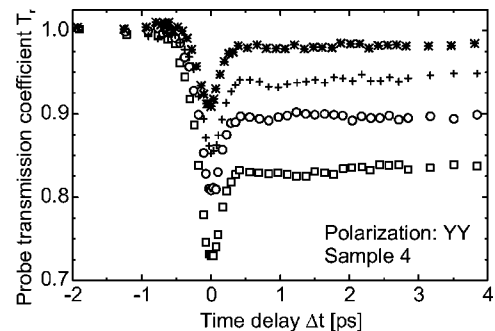

FIG. 5. Normalized transmission coefficient T_r for the probe pulse versus the time delay Δt for sample 4 and four different values of the pump intensity. The stars, crosses, circles, and squares correspond to $I_p^0 \simeq 43$, 68, 93, and 139 GW/cm^2, respectively.
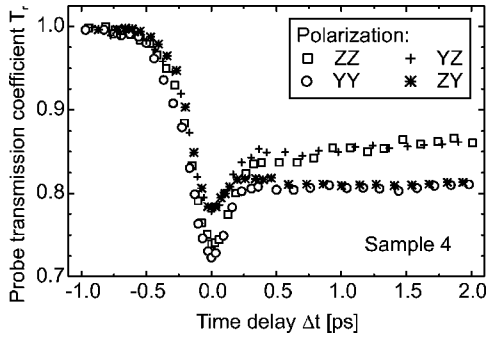
FIG. 6. Transmission coefficient T_r versus Δt for different pump and probe polarizations; the first and second characters of each pair in the inset (e.g., *YZ*) specify the orientation of the polarization vector of the pump and probe pulses, respectively.

This dependence is highly remarkable. It is characterized by a narrow dip (its temporal width is comparable with that of the pulses) followed by a quasipermanent section (plateau). Both the minimum and plateau values of $T_r(\Delta t)$ decrease nonlinearly with increasing pump intensity. One can see also that the decrease of the plateau T_r^{plat} with increasing I_p^0 occurs faster than that of the minimum value T_r^{min}.

The influence of the pump and probe polarizations on the probe transmission is illustrated by Fig. 6. It shows the dependence $T_r(\Delta t)$ for sample 4, $I_p^0 \simeq 105 \text{ GW/cm}^2$, and four different combinations of beam polarizations, including the cases of orthogonal polarizations.

The dip is more pronounced for parallel polarization of the pump and probe pulses (*ZZ* and *YY*); the influence of the orientation of the polarization plane is fairly weak. The plateau value of $T_r(\Delta t)$ is determined by the probe polarization; it is slightly larger for the *Z*-polarized probe beam.

In relatively thick samples the dependence $T_r(\Delta t)$ experiences distortions (see Fig. 7). The dip is noticeably asymmetric in this case and its temporal width is larger than that in Fig. 5. Despite the fact that the maximum value of q_p is about 60 in Fig. 7, the value $T_r^{min} \simeq 0.66$ is not much smaller than that in the case of $q_p \simeq 4$ ($T_r^{min} \simeq 0.74$) (see the data of Fig. 6).

Last, we have measured the dependences of the dip and plateau amplitudes on the pump absorption parameter $\beta_p I_p^0 d$.
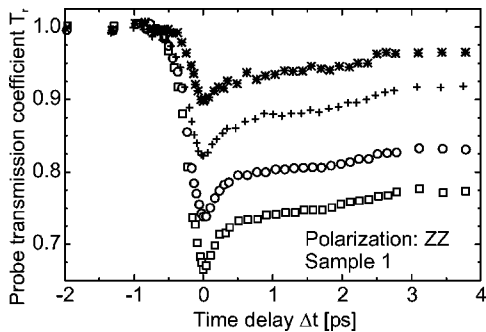

FIG. 7. Normalized transmission coefficient T_r for the probe pulse versus the time delay Δt for sample 1 ($d = 1$ mm) and four different values of the pump intensity. The stars, crosses, circles, and squares correspond to $I_p^0 \simeq 24$, 49, 101, and 147 GW/cm^2, respectively.
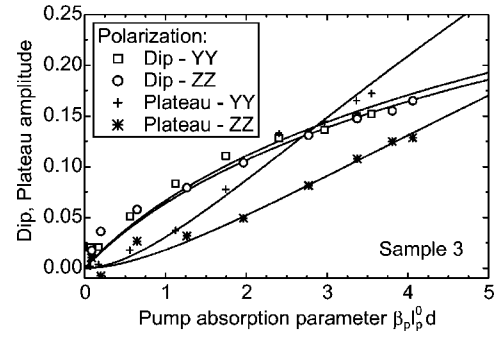

FIG. 8. Dependence of the dip and plateau amplitudes on the product $\beta_p I_p^0 d$ for sample 3 and two different pump-probe polarization states. The points are experimental data and the solid lines are theoretical fits.

It was done for thin (70 μm) samples where the dip shape is symmetric. The dip and plateau amplitudes are determined as $1 - T_r^{min} - \frac{1}{2}[1 - T_r(\Delta t = 2 \text{ ps})]$ and $1 - T_r(\Delta t = 2 \text{ ps})$, respectively.

The points in Fig. 8 show the corresponding experimental data for two different polarization cases *YY* and *ZZ*. One sees that the dip amplitude tends to saturate with increasing $\beta_p I_p^0 d$ while the plateau amplitude shows no saturation. The solid lines in Fig. 8 show a theoretical fit (see the next two subsections for details).

B. Modeling of probe transmission

The plateau section in the dependence $T_r(\Delta t)$ can be attributed to the absorption of the probe pulse by charge carriers (electrons and/or holes) that are excited via the pump-induced two-photon process. Recombination of the photoexcited carriers is not expected to occur on the picosecond time scale [1,22]. Some polarization dependence of the plateau value is explained by the crystal anisotropy.

The dip in the $T_r(\Delta t)$ curve represents a new effect. It contrasts with the effect of increasing probe intensity owing to coherent (parametric) pump-probe interactions which is known for a number of semiconductors [23–25]. The decrease of the probe pulse intensity in the presence of the pump pulse is obviously of a different origin. We attribute it to direct band-band transitions involving simultaneously pump and probe photons; their total energy ($\simeq 4.8$ eV) exceeds the width of the forbidden gap of LiNbO$_3$ ($\simeq 3.9$ eV). It is not surprising that identical polarizations of the pump and probe facilitate this two-photon process.

Since the dip and plateau are of different physical origins, we model them separately.

1. Shape of the dip

The instantaneous contribution to the pump-induced absorption at the probe wavelength λ_r can be characterized by the absorption coefficient $\alpha_r = \beta_r I_p$, where β_r is a new two-photon coefficient. The relevant linear evolution equation for the probe intensity I_r has the form [compare to Eq. (1)]

$$\left(\frac{\partial}{\partial x} + \frac{1}{v_r}\frac{\partial}{\partial t}\right)I_r = -\beta_r I_r I_p, \tag{5}$$

where $v_r = c/n_r$ is the probe pulse velocity and n_r is the refractive index at λ_r. Since $I_r \ll I_p$, the probe cannot influence the pump intensity distribution $I_p(x,r,t)$; the latter is given by Eq. (3).

To solve Eq. (5), it is useful to transfer from x and t to the independent variables $x' = x$ and $t' = t - xv_r^{-1}$; this means the transition into a coordinate frame moving with the probe pulse velocity. In the new variables Eq. (5) simplifies to

$$\partial I_r / \partial x' = -\beta_r I_r I_p. \tag{6}$$

After simple calculations we obtain from here the following explicit relation for the output intensity of the probe pulse $I_r^d = I_r(d,t,r)$ (in the x, t terms):

$$I_r^d = I_r(0, t - t_0, r)\exp\left[-\beta_r \int_0^d I_p(x, t - t_0, r)dx\right], \tag{7}$$

where $t_0 = d/v_r$ is the probe pulse traveling time and $I_r(0,t,r)$ is the input intensity for the probe.

Let the input profile of the probe beam be given by

$$I_r(0,t,r) = I_r^0 \exp\left[-\frac{(t - \Delta t)^2}{t_p^2} - \frac{r^2}{r_p^2}\right], \tag{8}$$

where Δt is the delay time between probe and pump pulses. It is assumed, in accordance with the experimental conditions, that the probe pulse duration and transverse width at the input are the same as those of the pump, compare with Eq. (2).

Using Eq. (3) and integrating $I_r(d,t,r)$ over the time t and the transverse coordinates y, z, one can calculate the normalized transmission coefficient of the probe pulse T_r. The shape of the function $T_r(\Delta t)$ is controlled by three dimensionless parameters: the known pump absorption parameter $q_p = \beta_p I_p^0 d$, the ratio β_r / β_p, and $\delta_0 = (v_p^{-1} - v_r^{-1})d/t_p = (n_p - n_r)d/ct_p$. The last parameter is responsible for the broadening and asymmetric distortions of the dip. In LiNbO$_3$, the difference $n_p - n_r$ is $\simeq 0.2$ for the ordinary waves (the YY case) and $\simeq 0.17$ for the extraordinary waves (the ZZ case) [26]. In both polarization cases, the parameter δ_0 can be estimated as $1/3$ for our thin (0.07 mm) samples and 5 for our thick (1 mm) sample.

We consider first the dip shape for the thin samples where the effects of broadening and distortion can be neglected in the leading approximation. By setting $v_p = v_r$, one can obtain from Eq. (7), after intermediate integrations,

$$T_r = \frac{e^{-(\Delta t/t_p)^2}}{\sqrt{\pi}aq_p}\int_{-\infty}^{\infty} e^{2s\Delta t/t_p}[(1 + q_p e^{-s^2})^a - 1]ds, \tag{9}$$

where $a = (\beta_p - \beta_r)/\beta_p$. As follows from here, T_r is an even function of Δt; i.e., the dip shape is symmetric.

In the limit of weak pump absorption, $q_p \ll 1$, Eq. (9) transforms into the following simple relation:

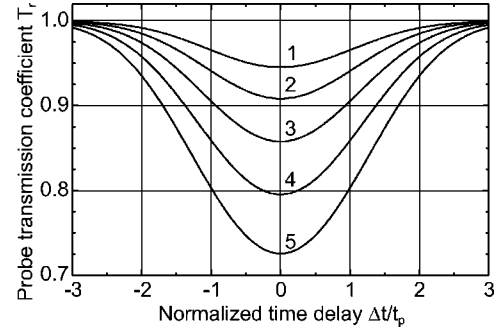FIG. 9. The normalized transmission coefficient T_r versus $\Delta t/t_p$ for $\beta_r / \beta_p = 0.2$ and $q_p = 1, 2, 4, 8$, and 16 (curves 1, 2, 3, 4, and 5, respectively).

$$T_r \simeq 1 - \frac{\beta_r I_p^0 d}{2\sqrt{2}}\exp\left[-\frac{(\Delta t)^2}{2t_p^2}\right]. \tag{10}$$

Thus we have a Gaussian-shaped dip for $T_r(\Delta t)$. Its temporal width is larger than that of the input pulses by a factor of $\sqrt{2}$. The amplitude of the dip, $1 - T_r(0)$, grows linearly with increasing pump intensity I_p^0 and probe absorption coefficient β_r.

Unfortunately, the field of applicability of the approximation of weak pump absorption is rather narrow. If $q_p \gtrsim 1$, the dip amplitude depends nonlinearly on I_p^0. Figure 9 shows the dependence of T_r on the normalized delay time $\Delta t/t_p$ plotted on the basis of Eq. (9) for $q_p = 1, 2, 4, 8$, and 16; the ratio β_r / β_p is set to be equal 0.2. One can see that the width of the dip gradually becomes larger with increasing $\beta_p I_p^0 d$ product. The shape of the dip is not Gaussian in the general case.

The dependence of the dip amplitude on the pump absorption parameter q_p is shown in Fig. 10 for four representative values of the ratio β_r / β_p. This dependence is linear only for $q_p \lesssim 1$; outside this range the dip amplitude experiences a strong saturation. The amplitude of the dip grows noticeably with increasing β_r / β_p ratio. Since the coefficient β_p is known from the pump absorption experiments, it is possible to estimate the value of β_r from the pump-probe experiments (see below).

Consider last the effects of broadening and distortion of the dip caused by the difference in the pump and probe velocities; these effects are expected to be significant for our
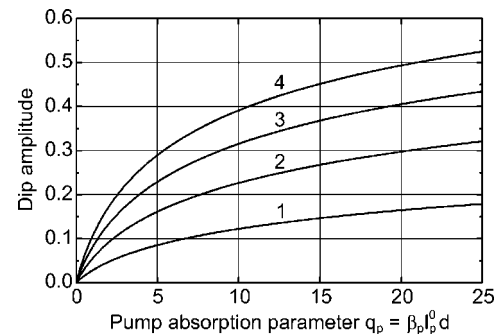

FIG. 10. Dependence of the dip amplitude on q_p; lines 1, 2, 3, and 4 are plotted for $\beta_r / \beta_p = 0.1, 0.2, 0.3$, and 0.4, respectively.
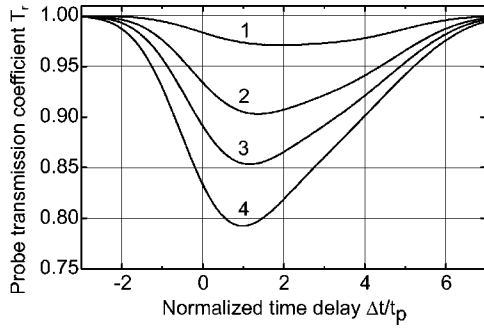
FIG. 11. The normalized transmission coefficient T_r versus $\Delta t/t_p$ for $d=1$ mm, $\beta_r/\beta_p=0.2$, and $\delta_0=5$. Curves 1, 2, 3, and 4 are plotted for $q_p=1$, 5, 10, and 20, respectively.

FIG. 12. Dependence of the plateau amplitude on the pump absorption parameter q_p; lines 1, 2, 3, 4, and 5 are plotted for $b=0.01$, 0.03, 0.06, 0.09, and 0.12, respectively.

thick (1 mm) sample. By keeping $v_p \neq v_r$ in Eq. (7), one can obtain the general relation

$$
T_r = \frac{1}{\sqrt{\pi}} \int_{-\infty}^{\infty} \exp[-(s-\Delta t/t_p)^2]
$$
$$
\times \int_0^1 \exp\left[-\frac{\beta_r}{\beta_p} \int_0^1 \frac{q_p f\,du}{q_p fu + \exp[(s-\delta_0 u)^2]}\right] df\,ds.
$$
$$(11)$$

In the limiting case $\delta_0=0$ two of three integrations can be performed analytically and we return to Eq. (9).

Figure 11 shows the shape of the dip for $\delta_0=5$ and several values of the pump intensity. One sees that the dip experiences a noticeable broadening and becomes asymmetric, its right wing being considerably longer than the left one. Qualitatively, these features are in good agreement with the experimental data for the 1-mm sample presented in Fig. 7. Furthermore, the dip amplitude is noticeably smaller in the thick sample under the condition that the values of $\beta_p I_p^0 d$ be the same for the thin and thick crystals. This feature is also in line with our experimental data (compare Figs. 5 and 7). Note that according to Fig. 11 the minimum of the transmission can occur after $\Delta t/t_p=0$. This is not in contradiction to our experiment (e.g., Fig. 7), because there $\Delta t/t_p$ was set to be zero at the minimum of the transmission.

2. Plateau amplitude

Since the pump excites carriers via direct two-photon transitions, it is able to induce an additional absorption for the probe. This pump-induced absorption is expected to remain until recombination of the photoexcited carriers occurs—i.e., at least on the picosecond scale.

We suppose that the two-photon absorption of the pump pulse results in generation of electron-hole pairs. The generation rate is $\alpha_p I_p/2\hbar\omega_p = \beta_p I_p^2/2\hbar\omega_p$, where $\hbar\omega_p$ is the energy of a single pump quantum. If N and P are the concentrations of photoexcited electrons and holes, respectively, we have, in terms of x',t' (in the moving coordinate frame),

$$
\frac{\partial N}{\partial t'} = \frac{\partial P}{\partial t'} = \frac{\beta_p I_p^2}{2\hbar\omega_p} = -\frac{1}{2\hbar\omega_p}\frac{\partial I_p}{\partial x'}. \qquad (12)
$$

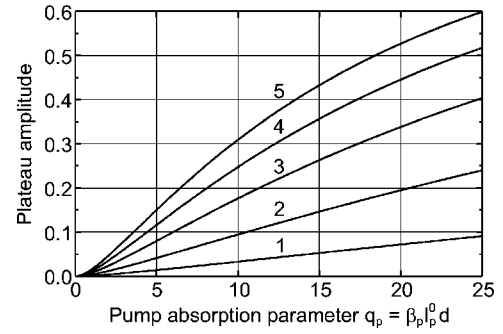Recombination processes are neglected in these equations.

In accordance with Eq. (12), the free-carrier contribution to the absorption coefficient for the probe α_r^f can be represented as

$$
\alpha_r^f(x',t') = -\frac{\sigma_r}{\hbar\omega_p}\frac{\partial}{\partial x'}\int_{-\infty}^{t'} I_p(x',t'')dt'', \qquad (13)
$$

where σ_r is the effective absorption cross section of the photoexcited carriers at the readout wavelength λ_r. Since the function $I_p(x',t')$ is known [see Eq. (3)] it is possible to calculate the above integral.

The probe intensity $I_r(x',t')$ obeys the equation $\partial I_r/\partial x' = -(\beta_r I_p + \alpha_r^f) I_r$ [compare to Eq. (5)]. Its solution has the form

$$
I_r = I_r(0,t')\exp\left[-\int_0^{x'} (\beta_r I_p + \alpha_r^f)dx''\right]. \qquad (14)
$$

The time dependence of I_r comes from the dependence of α_r^f, I_p, and $I_r(x=0)$ on t'.

Consider the case when the pump pulse has passed through; i.e., the instantaneous processes are over. This corresponds to the plateau value of the probe transmission. Mathematically, we have to set $I_p=0$ in Eq. (14) and $t'=\infty$ in Eq. (13); the value of α_r^f depends then only on x' (and r) but does not depend on t'. Using Eq. (8) for $I_r(0,t,r)$, it is not difficult now to calculate the plateau value of the transmission coefficient T_r^{plat},

$$
T_r^{plat} = \int_0^{\infty} \exp\left[-f - bq_p\left(\frac{\sqrt{\pi}}{2}e^{-f} - \int_0^{\infty}\frac{ds}{q_p + e^{f+s^2}}\right)\right]df, \qquad (15)
$$

where $b=2\sigma_r t_p/\hbar\omega_p\beta_p d$ is a new dimensionless parameter. The value of T_r^{plat} depends on two characteristic parameters q_p and b; only the first of them depends on the pump intensity I_p^0. Since the decrease of T_r is relatively small in the experiments and the parameter q_p is definitely larger than unity, it is reasonable to expect that $b \ll 1$.

Lines 1–5 in Fig. 12 show the dependence of the plateau amplitude, $1-T_r^{plat}$, on the pump absorption parameter $q_p = \beta_p I_p^0 d$ for five representative values of b. This amplitude grows quadratically for $q_p \lesssim 1$ and almost linearly for $1 \lesssim q_p \lesssim 15$. Its saturation with increasing q_p occurs rather

slowly. The behavior of the dip amplitude within the same interval (see Fig. 10) is different. Since the value of q_p is known from pump-absorption experiments, it is possible to estimate b and the cross section σ_r from the data of pump-probe experiments.

C. Comparison with experimental results and determination of probe absorption parameters

In accordance with the theory, our experiment shows that the dip profile is almost symmetric in the thin (70 μm) samples (see Figs. 5 and 9). According to the experiments, the ratio FWHM of the dip / FWHM of pump pulse ranges from $\simeq 1.7$ to $\simeq 2.1$ for the thin samples. The theory predicts the range 1.4–1.6 for this ratio. The difference is not large. It can be explained by an uncertainty of the measurements and some contribution originating from different pump and probe velocities. Considerable broadening of the dip and the noticeable asymmetry of its shape in the 1-mm sample, observed experimentally (see Fig. 7), are in a good qualitative agreement with theory (Fig. 11).

Figure 8 shows experimental data for the dependence of the dip and plateau amplitudes on the pump absorption parameter q_p, obtained for two different polarization cases, together with the theoretical fit. The fit parameters are the ratio β_r/β_p (for the dip amplitude) and $b = 2\sigma_r t_p/\hbar\omega_p\beta_p d$ (for the plateau amplitude). The agreement between theory and experiment is pretty good. Whereas the dip amplitude experiences a remarkable saturation with increasing q_p, the plateau amplitude shows no saturation within the experimental intensity range.

The ratio β_r/β_p deduced from the fit procedure is $\simeq 0.245$ for the YY case and $\simeq 0.235$ for the ZZ case. Thus, with an accuracy of (10–15)%, the value of β_r can be estimated as $\simeq 0.88$ cm/GW. The values of b can be estimated as $\simeq 0.237$ and $\simeq 0.138$ for the YY and ZZ cases, respectively. This gives, for the excitation cross section, $\sigma_{yy} \simeq 9.2 \times 10^{-18}$ cm^2 and $\sigma_{zz} \simeq 6.0 \times 10^{-18}$ cm^2. With an accuracy of $\simeq 10\%$ the above estimates are applicable to sample 3.

V. DISCUSSION

Below we discuss two important issues that are closely related to the results obtained.

General physical picture. According to the data of our collinear pump-probe experiments, the action of strong femtosecond pulses at 388 nm on LiNbO$_3$ meets the following physical picture.

(i) Initially, an instantaneous generation of free carriers takes place owing to direct two-photon processes. The corresponding nonlinear absorption coefficient is pretty high, $\beta_p \simeq 3.5$ cm/GW, so that the pump pulse experiences a strong attenuation even in relatively thin samples.

(ii) The pump-excited carriers do not experience recombination to the levels where they originate from at least on the time scale of tens of picoseconds. These carriers are responsible for the quasipermanent probe absorption (absorption plateau) at 776 nm.

(iii) When a weak probe pulse at 776 nm is overlapping

(in time and space) with a strong pump pulse, an additional instantaneous probe absorption, involving pump and probe photons, takes place. This nonlinear absorption causes a pronounced dip in the dependence of the probe transmission on the delay time between pump and probe pulses. The relevant nonlinear absorption coefficient is also pretty high, $\beta_r \simeq 0.88$ cm/GW.

Carrier relaxation. What happens with free carriers excited by pump pulses into the conduction and valence bands and what is the nature of carriers responsible for the plateau in the probe absorption?

The energy of two pump quanta, $2\hbar\omega_p \simeq 6.4$ eV, exceeds noticeably the energy gap of LiNbO$_3$ crystals ($\simeq 3.9$ eV). Therefore the band energy of photoexcited hot carriers exceeds considerably the thermal energy, $k_B T \simeq 0.026$ eV. At the first steps of establishment of the thermal equilibrium, energy relaxation and thermalization of hot carriers take place. The characteristic time of this process lies typically in the range $(10^{-13} - 10^{-12})$ s [1,22]. When the energy relaxation is over, the electrons (holes) occupy energy levels at the bottom (top) of the conduction (valence) band and/or shallow levels in the close vicinity of these bands. The subsequent recombination occurs much slower, typically during the time $\gtrsim 10^{-9}$ s. Details of the final relaxation stage depend greatly on the concentration and position of the energy levels in the forbidden energy gap. These levels can originate from doping and from partial disorder of the crystal structure.

The data $T_r(\Delta t)$ obtained in the thin samples (see Fig. 5) show no indication of an energy relaxation of hot carriers. No new temporal features with a characteristic scale essentially different from the pulse duration can be seen. This means that either the probe absorption cross section does not depend on the carrier energy or the time of energy relaxation is shorter than the pulse duration. The second possibility looks most probable and it does not contradict the above general estimates. If it is the case, shorter pulses are needed to monitor the energy relaxation. The asymmetry of the dip shape in the thick sample (see Fig. 7), which might, by itself, be interpreted as the effect of energy relaxation, is explained by the difference in the pump and probe velocities.

Most probably the pump-excited carriers, which are responsible for the plateau section of the probe transmission, occupy shallow levels near the conduction band. The presence of such levels, attributed usually to the structural Nb$_{\text{Li}}^{4+}$ defects of LiNbO$_3$ (small polarons), is known from pulse experiments on light-induced infrared absorption [20,27]. Recombination of such excited localized electrons occurs on the time scale $10^{-8} - 10^{-5}$ s and follows the stretched-exponential law typical for disordered materials.

VI. CONCLUSIONS

Two-photon absorption processes strongly affect the propagation of high-power femtosecond pump pulses in LiNbO$_3$ at 388 nm. The corresponding nonlinear absorption coefficient, $\beta_p \simeq 3.5$ cm/GW, does not show a strong dependence on light polarization and crystal doping.

Strong pump pulses induce instantaneous and quasipermanent contributions to probe absorption at 776 nm. The

instantaneous contribution is due to two-photon processes with participation of pump and probe photons; the corresponding nonlinear absorption coefficient $\beta_r \simeq 0.88$ cm/GW is not polarization sensitive. The quasipermanent contribution is due to probe absorption by pump-excited carriers; the absorption cross section σ_r is about 9.2×10^{-18} cm^2 and 6.0×10^{-18} cm^2 for the light polarization vector perpendicular and parallel to the polar axis, respectively.

The time of hot-carrier relaxation is expected to be shorter than 0.1 ps for the excitation wavelength 388 nm.

Strong nonlinear absorption effects will be important also for femtosecond pulse recording of spatial gratings in LiNbO$_3$.

[1] A. Othonos, J. Appl. Phys. **83**, 1789 (1998).

[2] A. McClelland, V. Fomenko, and E. Borquet, J. Phys. Chem. B **108**, 3789 (2004).

[3] T. Sjodin, H. Petek, and H. L. Dai, Phys. Rev. Lett. **81**, 5664 (1998).

[4] R. DeSalvo, A. A. Said, D. J. Hagan, E. W. Van Strylnd, and M. Sheik-Bahae, IEEE J. Quantum Electron. **QE-32**, 1324 (1996).

[5] A. Dragonmir, J. G. Mclnerney, and D. N. Nikogosyan, Appl. Opt. **41**, 4365 (2002).

[6] D. von der Linde, A. M. Glass, and K. F. Rodgers, Appl. Phys. Lett. **25**, 155 (1974).

[7] C.-T. Chen, D. M. Kim, and D. von der Linde, Appl. Phys. Lett. **34**, 321 (1979).

[8] A. L. Smirl, K. Bohnert, G. C. Valley, R. A. Mullen, and T. F. Boggess, J. Opt. Soc. Am. B **6**, 606 (1989).

[9] M. Ewart, I. Biaggio, M. Zgonik, and P. Günter, Phys. Rev. B **49**, 5263 (1994).

[10] L. Solymar, D. J. Webb, and A. Grunnet-Jepsen, *The Physics and Applications of Photorefractive Materials* (Clarendon Press, Oxford, 1996).

[11] K. Buse, Appl. Phys. B: Lasers Opt. **64**, 391 (1997).

[12] *Holographic Data Storage*, edited by H. J. Coufal, D. Psaltis, and G. T. Sincerbox (Springer, Berlin, 2000).

[13] *Infrared Holography for Optical Communications*, edited by P. Boffi, D. Piccinin, and M. C. Ubaldi (Springer, Berlin, 2003).

[14] M. Centini, C. Sibilia, M. Scalora, G. D'Aguanno, M. Berto-lotti, M. J. Bloemer, C. M. Bowden, and I. Nefedov, Phys. Rev. E **60**, 4891 (1999).

[15] V. Leyva, G. A. Rakuljic, and B. O'Conner, Appl. Phys. Lett. **65**, 1079 (1994).

[16] M. M. Fejer, G. A. Magel, D. H. Jundt and R. L. Byer, IEEE J. Quantum Electron. **28**, 2631 (1992).

[17] R. Müller, M. T. Santos, L. Arizmendi, and J. M. Cabrera, J. Phys. D **27**, 241 (1994).

[18] S. Breer and K. Buse, Appl. Phys. B: Lasers Opt. **66**, 339 (1998).

[19] D. N. Nikogosyan, *Properties of Optical and Laser-Related Materials* (Wiley, New York, 1997).

[20] F. Jermann and J. Otten, J. Opt. Soc. Am. B **10**, 2085 (1993).

[21] O. Beyer, D. Maxein, K. Buse, B. Sturman, H. T. Hsieh, and D. Psaltis, Opt. Lett. **30**, 1366 (2005).

[22] K. Seeger, *Semiconductor Physics* (Springer, New York, 1973).

[23] H. J. Eichler, P. Günter, and D. W. Pohl, *Laser-Induced Dynamic Gratings* (Springer-Verlag, Berlin, 1986).

[24] C. J. Kennedy, J. C. Matter, A. L. Smirl, H. Weiche, F. A. Hopf, S. V. Pappu, and M. O. Scully, Phys. Rev. Lett. **32**, 419 (1974).

[25] C. V. Shank and D. H. Auston, Phys. Rev. Lett. **34**, 479 (1975).

[26] U. Schlarb and K. Betzler, J. Appl. Phys. **73**, 3472 (1993).

[27] D. Berben, K. Buse, S. Wevering, P. Herth, M. Imlau, and Th. Woike, J. Appl. Phys. **87**, 1034 (2000).